Modeling the Transition between Localized and Extended Deposition in Flow Networks through Packings of Glass Beads

Gess Kelly, Navid Bizmark, Bulbul Chakraborty, Sujit S. Datta, and Thomas G. Fai

Modeling the Transition between Localized and Extended Deposition in Flow Networks through Packings of Glass Beads

Gess Kelly[1], Navid Bizmark[3,4], Bulbul Chakraborty[1], Sujit S. Datta[3], and Thomas G. Fai[2*]

[1]*Martin A. Fisher School of Physics, Brandeis University, Waltham, MA 02453*
[2]*Mathematics Department & Volen Center for Complex Systems, Brandeis University, Waltham, MA 02453*
[3]*Department of Chemical and Biological Engineering,*
Princeton University, Princeton, NJ 08544, USA and
[4]*Princeton Institute for the Science and Technology of Materials,*
Princeton University, Princeton, NJ 08540, USA
(Dated: February 28, 2023)

We use a theoretical model to explore how fluid dynamics, in particular, the pressure gradient and wall shear stress in a channel, affect the deposition of particles flowing in a microfluidic network. Experiments on transport of colloidal particles in pressure-driven systems of packed beads have shown that at lower pressure drop, particles deposit locally at the inlet, while at higher pressure drop, they deposit uniformly along the direction of flow. We develop a mathematical model and use agent-based simulations to capture these essential qualitative features observed in experiments. We explore the deposition profile over a two-dimensional phase diagram defined in terms of the pressure and shear stress threshold, and show that two distinct phases exist. We explain this apparent phase transition by drawing an analogy to simple one-dimensional models of aggregation in which the phase transition is calculated analytically.

I. INTRODUCTION

Deposition and aggregation of fine particles in microfluidic networks and porous media play an important role in various natural and industrial processes such as water purification, geotextile filtration, applications in precision drug delivery and similar biomedical tasks, transport of microplastics, environmental cleanups, groundwater pollutant removal, oil recovery, and transport of nanomaterials for groundwater aquifer remediation [1–7] [8–11]. For example, in filtration processes, understanding of the deposition dynamics of colloidal particles plays a significant role in improving filter efficiency via reducing filter fouling [12–14]. Observations from [15] indicate that, regardless of the charge of the colloidal particles flowing in the bead network, applying lower pressures across the system leads to localized deposition under various conditions. This may suggest that irrespective of the exact local clogging mechanism (e.g., bridging versus aggregation [16]), the interplay of hydrodynamic variables in these systems controls the resulting deposition profile. We focus on the role of applied pressure difference ΔP as one of the key variables motivated by the experimental design in [15] and the wall shear stress τ_w, which has been shown in past studies to play an important role in erosion [17–19]. Here, the shear stress at the wall τ_w refers to the shear stress experienced by colloidal particles deposited on the walls of the packing. We follow the approach of [19] to capture the role of the shear stress threshold τ, a material parameter that describes the threshold shear stress at the wall above which fluid flow erodes the deposited particles

from the walls. Table S1 in the Supplementary Materials contains representative parameter values. Throughout the text, we use a hat notation, e.g., $\Delta \hat{P}$, to denote the corresponding variables, e.g., ΔP, that are normalized by a set value relevant to the experimental system. Table S2 in the Supplementary Material contains additional details.

Our specific system of interest is motivated by recent experiments from [15], in which a constant pressure difference ΔP applied to a packing of disordered glass beads of length L drives a fluid flow containing a suspension of colloidal particles. These experiments show that at larger pressure differences, the profile of particles deposited on the solid matrix extends uniformly along the length of the packing, while at lower pressure, the particles deposit locally at the inlet where they are injected into the system. Here, we develop a mathematical model to explain how the pressure difference influences the deposition profile.

Past studies of simple aggregation models [14, 21] motivate us to explore the phase space of shear stress threshold $\hat{\tau}$ and pressure difference $\Delta \hat{P}$. In particular, Majumdar et al. [21] consider minimal systems and lattice toy models in which discrete masses diffuse at a constant unit rate, which normalizes the overall timescale. Multiple masses may aggregate at lattice sites after diffusion, and units of masses erode (chip away) from blocks at a constant chipping rate w. Physically, chipping corresponds to single-particle dissociation in processes such as polymerization and competes with coalescence. In this simplest case, they work with two independent variables, the chipping rate w and mass density ρ, that remain constant and determine the behavior of the system at steady state. They explore the phase space consisting of the mass density ρ and chipping rate w and show that these finite systems exhibit two distinct phases at steady state, only one of which involves an infinite aggregate. One im-
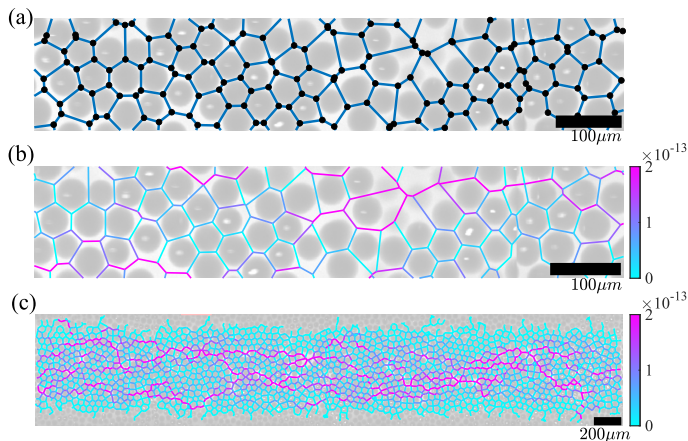
FIG. 1. We use a network approach to model the bead packing
here shown in the absence of particles. (a) We skeletonize
the image of the packing, and then generate a network. The
edges of the network represent the channels through which
fluid may flow in the packing and the nodes represent the
junctions where these channels meet. (b) We obtain the flow
rates in the channels by applying the Kirchhoff's laws [20].
(c) Zoomed-out view showing the network as a whole. The
color in (b) and (c) shows the magnitude of the channel flow
rates in SI units (m^3/s). (a) and (b) have the same scale bar.
The grey background shows the experimental micrograph of
the beads.

portant difference between the toy model and our study
is the fixed density or constant total mass with periodic
boundary conditions in contrast to our model where there
is a flux of particles into and out of the system.

We formulate the fluid flow through the packings by
applying the hydraulic analogy to the network of channels
extracted from the bead packing images. Using our net-
work model and deposition and erosion laws, we demon-
strate a similar transition in the normalized shear stress
threshold $\hat{\tau}$ and pressure $\Delta\hat{P}$ phase space. Motivated
by these simple toy models of aggregation and fragmen-
tation explored in previous studies [21, 22], we explore
the model phase space spanned by two dimensionless pa-
rameters, and identify a transition between extended and
localized deposition regimes in terms of the key parame-
ters of pressure difference and shear stress threshold [23].

II. METHODS

We use a graph- or network-based approach [24, 25]
to model the porous network created by the beads as
shown in FIG. 1(a). The idea of modeling a porous sys-
tem as a network has been studied previously [26–28].
For instance, past studies have demonstrated the effec-
tiveness of a network-based approach by highlighting the
role of disorder on the flow distribution in porous media
[29]. We use images of two-dimensional (2D) slices of
the three-dimensional (3D) packing. We then generate
the model network based on these images. Because of

the expected differences between the flow in 2D and 3D,
we do not expect to quantitatively recover all aspects of
the experiments. In such network models, each pore or
channel is typically represented by an edge in a network
representing the whole porous system (see FIG. 1.(a)).
Each edge may be weighted in terms of its conductance
and the nodes of the network represent junctions between
the edges. Assuming we have an incompressible fluid, the
inflow and outflow of particles and fluid must be equal
to respect mass conservation. In our system of interest,
boundary junctions at the inlet and outlet are subject to
two pressures held constant for the duration of the ex-
periment. To solve for the resulting channel flow rates,
as shown in FIG. 1 (b) and (c), we apply Kirchhoff's
circuit laws. For each channel, we estimate the channel
length l and diameter d from the image of the network to
calculate the channel conductance g, which is defined as
the proportionality constant between the volumetric flow
rate through a given channel and the pressure difference
across the channel given by the Hagen-Poiseuille law [20]:

$$g = \frac{\pi d^4}{128\eta l},\tag{1}$$

where η is the dynamic viscosity. The resolution of the
image in FIG. 1 tends to be lower along the boundaries
and our image processing does not accurately identify a
significant portion of the channels. We use the largest
connected component of the model network, which is in
the interior of the packing. For this reason we neglect
the upper and lower boundaries. More details regard-
ing channel flow rate calculations can be found in the
Supplementary Material. The total flow rate is of order
$10^{-10}\,m^3/s$ once we account for the depth of the three-
dimensional system.

To capture the stochastic effects, we use agent-based
modeling to model the particles as they deposit and erode
within the network. This distinguishes our study from a
closely related previous model of erosion in networks in
which differential equations are used to predict how ero-
sion changes the width of the channels in the network
[28]. Another difference is our assumption that the glass
beads that form the network remain fixed over the course
of the simulation. Consequently, while the deposited par-
ticles may erode in our simulation, the channels them-
selves do not erode. Because initially the channel does
not contain any deposited particles, and since erosion
only occurs through removal of particles, the channel
width cannot grow beyond its initial value.

Particles enter the system from the inlet at constant
time intervals. This is a discrete approximation to the
experiments, in which the particles are injected continu-
ously at a constant volume fraction. This is also differ-
ent from the conserved-mass aggregation models of [21]
where the density is constant. As particles deposit in the
network during the simulations, they cause a decrease
in the width of the channels, which may eventually lead
to larger topological changes when the number of de-
posited particles surpasses the channel capacity, i.e., clog-

ging. We assume that each time a particle is deposited (eroded), it causes a uniform reduction (increase) in the channel width. This assumption is motivated by the separation of length scales in the experiments, in which the glass bead diameter is approximately $40\mu m$ so that the particle-to-bead size ratio is approximately 0.03.

We follow the suggested model of [19] when defining the deposition rate λ_d and erosion rate λ_e of particles using shear stress thresholds: the deposition threshold τ_d and erosion threshold τ_e, and shear stress at the channel wall τ_w. Since we are interested in cases where both deposition and erosion occur, to reduce the number of independent parameters, here, we assume that the wall shear stress thresholds for deposition and erosion are equal, i.e., $\tau_d = \tau_e = \tau$, so that the deposition rate and erosion rate equations are:

$$\lambda_d(\tau) = \begin{cases} \kappa_d(\tau - \tau_w), & \text{if } \tau_w < \tau \\ 0, & \text{otherwise,} \end{cases} \quad (2)$$

and

$$\lambda_e(\tau) = \begin{cases} \kappa_e(\tau_w - \tau), & \text{if } \tau_w > \tau \\ 0, & \text{otherwise.} \end{cases} \quad (3)$$

Here, κ_d and κ_e are deposition and erosion coefficients that depend on solid properties, respectively [19]. We note that τ_w depends on the imposed fluid flow conditions, whereas τ_d and τ_e reflect the material properties of the deposited particles independent of flow. In particular, a larger τ requires a larger wall shear stress for particle erosion. We run the simulation for multiple values of $\Delta\hat{P}$ and $\hat{\tau}$, keeping all other parameters, including the length of the medium $\hat{L}$, constant.

III. RESULTS

In both experiments and simulations, $F(x)$ the cumulative distribution function of deposited particle position varies significantly between the localized and extended deposition regimes. We approximate this function as

$$F(x) \approx N(X \le x)/N, \quad (4)$$

where $N(X \le x)$ is the number of deposited particles at position less than or equal to x, and N is the the total number of deposited particles. The position along the direction of the flow x is normalized by the full length of the medium. As shown in FIG. 2, when the deposition is localized, $F(x)$ attains a value near 1 for $x < 0.5$, showing that most of the deposited particles are close to the inlet. In contrast, in the extended deposition case, $F(x)$ has a more linear form with $F(x) \approx 0.5$ when $x = 0.5$. More information regarding the normalization constants is included in Table S2 in Supplementary Material.

Our simulations reveal that for each wall shear stress threshold $\hat{\tau}$, there exists a critical pressure $\Delta\hat{P}_c$ that separates the localized and extended regimes (FIG. 3). For
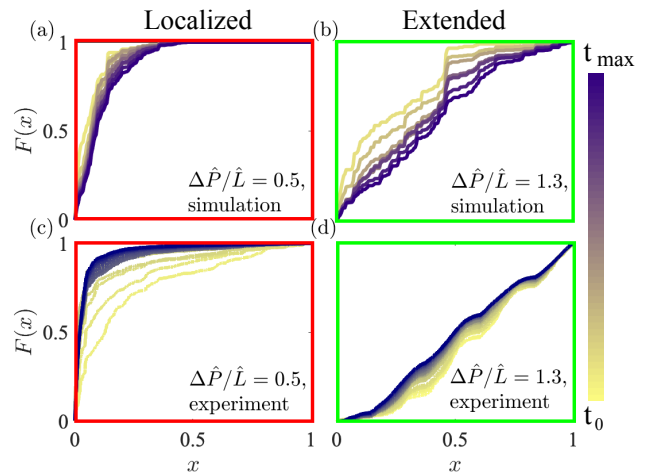

FIG. 2. The cumulative probability distribution function of deposition along the flow direction $F(x)$ for the localized and the extended case obtained by simulation and experiment show a similar qualitative behavior. The darker colors indicate later times. The position along the direction of the flow x is normalized by the total length of the medium. The labels indicate the normalized pressure gradient.

a specific value of $\hat{\tau}$, choosing $\Delta\hat{P}$ larger (smaller) than the critical value leads to extended (localized) deposition. To find the critical pressure $\Delta\hat{P}_c$ for a given $\hat{\tau}$, we vary $\Delta\hat{P}$ in the simulation while keeping all other parameters constant. As we decrease $\Delta\hat{P}$, the percentage of the deposited particles in the first half of the system increases. We mark $\Delta\hat{P}_c$ as the smallest $\Delta\hat{P}$ when the deposition is localized. FIG. 4 visualizes $\Delta\hat{P}_c$ for various pressure values and how the two regimes of localized and extended deposition are separated in the normalized shear stress threshold and pressure phase space. This behavior is similar to the phase transitions observed in simple mass aggregation models on lattice sites, with shear stress and pressure appearing on the corresponding axes of the phase diagram as the chipping rate and density in the chipping and aggregation model [21, 30]. The solid curve in FIG. 4 is the best power law fit motivated by the power law relation between the model parameters in [21]. In particular, we fit to a function of the form $ax^b + c$.

Majumdar et al. use the steady-state mass distribution to study the behavior and dynamical phase transition of their model, in which the distribution transitions from an exponential to a power-law with an aggregate [21]. Our numerical investigation of the mass distribution has revealed signs of a similar behavior when transitioning between the extended and localized phases. However, accurate classification of the transition seen in our model requires a more rigorous study of the critical point. Identifying the transition point in complex non-equilibrium systems such as ours where a free energy description of the system does not exist is a difficult task, and as a first step, one may simplify some of the complexities of the system to map it to other solvable models.
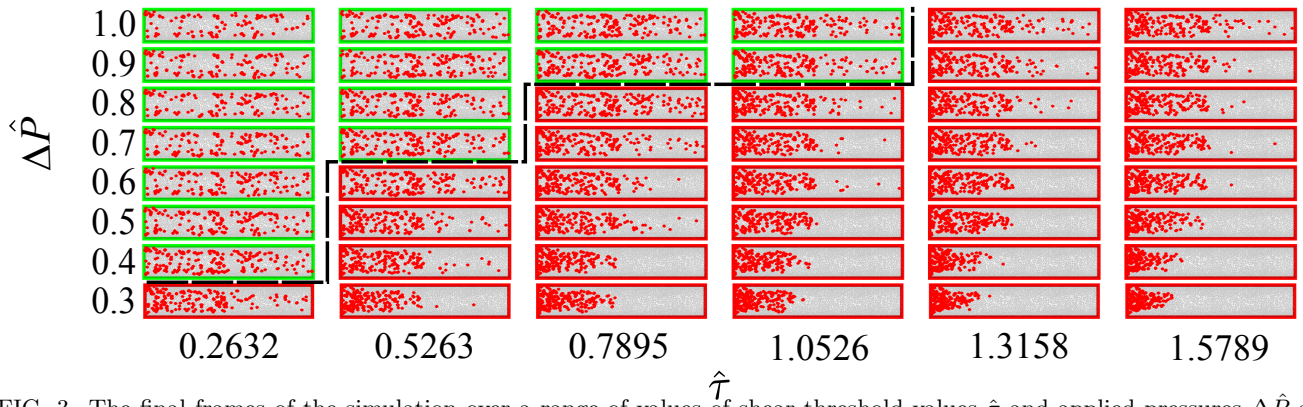
FIG. 3. The final frames of the simulation over a range of values of shear threshold values $\hat{\tau}$ and applied pressures $\Delta\hat{P}$ show a clear separation between the localized and extended deposition regimes similar to experimental observations in [15]. The dashed line serves to guide the eye.
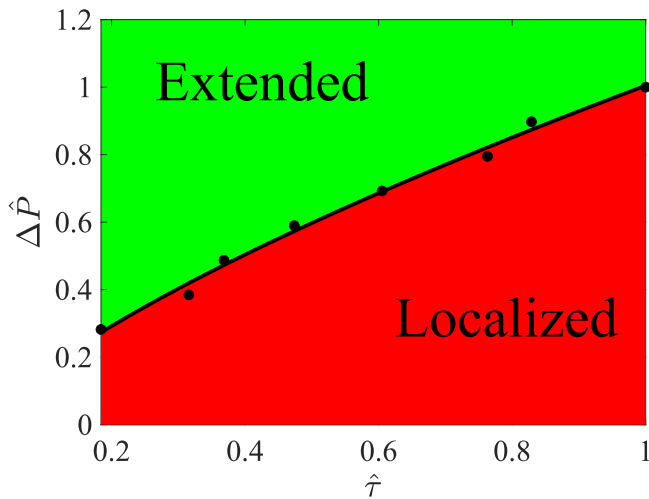

FIG. 4. In the parameter space of normalized pressure $\Delta\hat{P}$ and shear stress threshold $\hat{\tau}$, a boundary separates the two regimes of localized and extended deposition, reminiscent of the phases in [21]. The filled circles show the critical values of pressure P_c at which the transition to the localized phase occurs in simulations. The solid line corresponds to the best fit $\Delta\hat{P} = 1.04\hat{\tau}^{0.71} - 0.04$. The hat notation used here denotes normalization by the maximum value.

In the experiments, one of the tunable parameters is $\Delta\hat{P}$. We further assume that $\hat{\tau}$ is an independent parameter that depends on fluid, particle, and pore network properties. Given a system with a fixed $\hat{\tau}$, we expect localized deposition at lower $\Delta\hat{P}$, and extended deposition at higher $\Delta\hat{P}$ for the same network as seen in experiments [15] and simulations. FIG. 3 supports this reasoning. For particles with a given shear stress threshold $\hat{\tau}$, as we increase $\Delta\hat{P}$, a smaller percentage of deposition occurs near the inlet of the medium, consistent with the experimental findings. In the figure, the red borders indicate localized deposition, as defined by comparison to a representative experiment, and the green border indicates extended deposition. More details on categorizing localized and extended deposition are found in the Sup-

plementary Material. In the SM, we also demonstrate that this transition occurs over a range of sizes. The hat notation used here denotes normalization by the maximum value. The programming scripts used in generating the simulations discussed in this section are accessible on GitHub [31].

IV. DISCUSSION

Capturing the dynamics of deposition in porous media and microfluidic systems has wide implications in filtration studies. Understanding what leads to localized deposition helps in improving filter efficiency [26]. Experiments such as [15] provide more insight into the influence of global system hydrodynamics on uniformity of deposition profiles. Our theoretical model successfully captures the behavior observed in the experiments in [15]. Our network-based approach and simple model of shear-based deposition and erosion reveal a transition from the localized to extended regime in the phase space of shear stress threshold and pressure in colloidal transport within packings of beads. Given a system of beads, there exists a critical pressure above which the deposition profile becomes increasingly more uniform (see FIG. 4). This transition from the localized to extended regime is similar to what has been observed in previous studies of simple lattice models of aggregation [21]. The observation in similarities between these models of aggregation and our current model leads us to believe such analogies may be present in other systems, as well, where the key variables may be different. Future applications to other systems including filtration may examine and identify what variables control the phase transition in the system.

Our model may be thought of as a two-dimensional inhomogeneous asymmetric expansion of the aggregation toy model in [21]. Uncovering the limitations to this analogy requires a careful analysis. One important distinction between the two models concerns the boundary conditions. In the toy model, the total mass is constant, whereas in our model, there is a regular influx of parti-

cles into the system and particles may exit at the outlet boundary. Some other relevant models that allow an influx of particles include the aggregation-chipping model with open boundary conditions [32] and totally asymmetric simple exclusion (or inclusion) processes on networks [33, 34]. In our case, the direction of flow makes the model asymmetric, and although the asymmetric aggregation toy model also shows a phase transition in two dimensions, it belongs to a different universality class [30, 35]. Moreover, Rajesh et al. have shown that small tweaks such as making the deposition rate mass-dependent lead to different models with no phase transitions [36]. In our case, we assume identical particles with the same laws for deposition and erosion that do not explicitly depend on mass of individual particles; however, the flow, deposition, and erosion rates may change with time and differ for each channel. These differences lead to spatial bias and signs of channelization [19, 28, 37] where particles frequent a few paths rather than all paths in the system. Studies suggest in real world applications of the model, the erosion threshold and rate may depend on particle-particle interactions and spatial distribution of particles [37], similar to a mass-dependent law. Past studies considering the role of particle interactions in deposition report that strong particle interactions lead to a decrease in the transient flow rate [8]. We hypothesize that this decrease would lead to a lower effective local shear stress at the channel walls and hence a more localized deposition profile. Since particles act as agents in the model and simulations, adding interactions would be a possible expansion of the model in the future.

We note that, although the model is successful in capturing the essential behavior of the system, some details regarding the clogging mechanism are lost due to coarse-graining. This is most apparent in FIG. 2 in which the deposition appears to become more localized over time in experiments in contrast to simulations. It would be interesting to explore what leads to this difference in experiment and simulation observations by expanding the model to three dimensions. Additionally, one may expand (2) and (3) to consider an *overlap* region such that $\tau_e < \tau_d$ where for some values of wall shear stress, both deposition and erosion occur, or a *gap* region $\tau_d < \tau_e$ where for some values of wall shear stress, neither deposition nor erosion occur similar to the generalizations in [19].

V. ACKNOWLEDGEMENTS

[1] J. Linkhorst, T. Beckmann, D. Go, A. J. C. Kuehne, and M. Wessling, Microfluidic colloid filtration, Scientific reports **6**, 22376 (2016).

[2] Y. Faure, A. Baudoin, P. Pierson, and O. Plé, A contribution for predicting geotextile clogging during filtration of suspended solids, Geotextiles and geomembranes **24**, 11 (2006).

[3] C. Kleinstreuer, J. Li, and J. Koo, Microfluidics of nanodrug delivery, International Journal of Heat and Mass Transfer **51**, 5590 (2008), biomedical-Related Special Issue.

[4] A. Al Harraq and B. Bharti, Microplastics through the lens of colloid science, ACS Environmental Au **2**, 3 (2022).

[5] X. Zhao, W. Liu, Z. Cai, B. Han, T. Qian, and D. Zhao, An overview of preparation and applications of stabilized zero-valent iron nanoparticles for soil and groundwater remediation, Water Research **100**, 245 (2016).

[6] S. R. Kanel, J.-M. Grenèche, and H. Choi, Arsenic(v) removal from groundwater using nano scale zero-valent iron as a colloidal reactive barrier material, Environmental Science & Technology **40**, 2045 (2006), pMID: 16570634.

[7] T. Phenrat, H.-J. Kim, F. Fagerlund, T. Illangasekare, R. D. Tilton, and G. V. Lowry, Particle size distribution, concentration, and magnetic attraction affect transport of polymer-modified fe0 nanoparticles in sand columns, Environmental Science & Technology **43**, 5079 (2009), pMID: 19673310.

[8] E. S. Boek, H. K. Ladva, J. P. Crawshaw, and J. T. Padding, Deposition of colloidal asphaltene in capillary flow: Experiments and mesoscopic simulation, Energy & Fuels **22**, 805 (2008), https://doi.org/10.1021/ef700670f.

[9] E. S. Boek, T. F. Headen, and J. T. Padding, Multi-scale simulation of asphaltene aggregation and deposition in capillary flow, Faraday Discuss. **144**, 271 (2010).

[10] E. S. Boek, A. D. Wilson, J. T. Padding, T. F. Headen, and J. P. Crawshaw, Multi-scale simulation and experimental studies of asphaltene aggregation and deposition in capillary flow, Energy & Fuels **24**, 2361 (2010), https://doi.org/10.1021/ef9010059.

[11] K. A. Lawal, J. P. Crawshaw, E. S. Boek, and V. Vesovic, Experimental investigation of asphaltene deposition in capillary flow, Energy & Fuels **26**, 2145 (2012), https://doi.org/10.1021/ef201874m.

[12] N. Delouche, A. B. Schofield, and H. Tabuteau, Dynamics of progressive pore clogging by colloidal aggregates, Soft matter. **16**, 9899 (2020-11-11).

[13] A. Cirillo, G. Tomaiuolo, and S. Guido, Membrane fouling phenomena in microfluidic systems: From technical challenges to scientific opportunities, Micromachines. **12** (2021-7-13).

[14] M. P. Dalwadi, I. M. Griffiths, and M. Bruna, Understanding how porosity gradients can make a better filter using homogenization theory, Proceedings of the Royal

Society. A, Mathematical, physical, and engineering sciences **471**, 1 (2015).

[15] N. Bizmark, J. Schneider, R. D. Priestley, and S. S. Datta, Multiscale dynamics of colloidal deposition and erosion in porous media, Science advances **6** (2020).

[16] E. Dressaire and A. Sauret, Clogging of microfluidic systems, Soft matter **13**, 37 (2016).

[17] L. Ristroph, M. N. J. Moore, S. Childress, M. J. Shelley, and J. Zhang, Sculpting of an erodible body by flowing water, Proceedings of the National Academy of Sciences - PNAS **109**, 19606 (2012).

[18] N. Schorghofer, B. Jensen, A. Kudrolli, and D. H. Rothman, Spontaneous channelization in permeable ground: theory, experiment, and observation, Journal of fluid mechanics **503**, 357 (2004).

[19] R. Jäger, M. Mendoza, and H. Herrmann, Channelization in porous media driven by erosion and deposition, Physical review. E **95**, 013110 (2017).

[20] H. Bruus, *Theoretical microfluidics*, Oxford master series in physics ; 18 (Oxford University Press, Oxford, 2007).

[21] S. N. Majumdar, S. Krishnamurthy, and M. Barma, Nonequilibrium phase transitions in models of aggregation, adsorption, and dissociation, Physical review letters **81**, 3691 (1998).

[22] R. Rajesh and S. N. Majumdar, Exact phase diagram of a model with aggregation and chipping, Physical review. E, Statistical physics, plasmas, fluids, and related interdisciplinary topics **63**, 361141 (2001).

[23] There are different combinations of parameters (such as flow rate and pressure) that one could potentially choose, but as long as there is a way to map from one to the other, they are expected to be equivalent.

[24] B. Bollobás, *Modern graph theory*, Graduate texts in mathematics ; 184 (Springer, New York, 1998).

[25] A. Barrat, M. Barthélemy, and A. Vespignani, *Dynamical Processes on Complex Networks* (Cambridge University Press, 2008).

[26] I. Griffiths, A. Kumar, and P. Stewart, A combined network model for membrane fouling, Journal of colloid and interface science **432**, 10 (2014).

[27] S. Redner, Fractal and multifractal scaling of electrical conduction in random resistor networks, in *Mathematics of Complexity and Dynamical Systems*, edited by R. A. Meyers (Springer New York, New York, NY, 2011) pp. 446–462.

[28] A. Zareei, D. Pan, and A. Amir, Temporal evolution of erosion in pore networks: From homogenization to instability, Phys. Rev. Lett. **128**, 234501 (2022).

[29] K. Alim, S. Parsa, D. A. Weitz, and M. P. Brenner, Local pore size correlations determine flow distributions in porous media, Physical review letters **119**, 144501 (2017).

[30] S. N. Majumdar, S. Krishnamurthy, and M. Barma, Nonequilibrium phase transition in a model of diffusion, aggregation, and fragmentation, Journal of statistical physics **99**, 1 (2000).

[31] Modeling the transition between localized and extended deposition in flow networks through packings of glass beads, `https://github.com/gsiraji/particleDeposition`.

[32] H. Sachdeva, M. Barma, and M. Rao, Condensation and intermittency in an open-boundary aggregation-fragmentation model, Phys. Rev. Lett. **110**, 150601 (2013).

[33] I. Neri, N. Kern, and A. Parmeggiani, Totally asymmetric simple exclusion process on networks, Phys. Rev. Lett. **107**, 068702 (2011).

[34] S. Reuveni, O. Hirschberg, I. Eliazar, and U. Yechiali, Occupation probabilities and fluctuations in the asymmetric simple inclusion process, Phys. Rev. E **89**, 042109 (2014).

[35] R. Rajesh and S. Krishnamurthy, Effect of spatial bias on the nonequilibrium phase transition in a system of coagulating and fragmenting particles, Phys. Rev. E **66**, 046132 (2002).

[36] R. Rajesh, D. Das, B. Chakraborty, and M. Barma, Aggregate formation in a system of coagulating and fragmenting particles with mass-dependent diffusion rates, Physical review. E, Statistical, nonlinear, and soft matter physics **66**, 056104 (2002).

[37] A. Kudrolli and X. Clotet, Evolution of porosity and channelization of an erosive medium driven by fluid flow, Phys. Rev. Lett. **117**, 028001 (2016).

[38] J. Rommes and W. H. A. Schilders, Efficient methods for large resistor networks, IEEE Transactions on Computer-Aided Design of Integrated Circuits and Systems **29**, 28 (2010).

[39] D. Zhang and G. Lu, Review of shape representation and description techniques, Pattern Recognition **37**, 1 (2004).

[40] H. Chatbri, K. Kameyama, and P. Kwan, A comparative study using contours and skeletons as shape representations for binary image matching, Pattern Recognition Letters **76**, 59 (2016), special Issue on Skeletonization and its Application.

[41] Z. Jiang, K. Wu, G. Couples, M. I. J. van Dijke, K. S. Sorbie, and J. Ma, Efficient extraction of networks from three-dimensional porous media, Water resources research **43**, W12S03 (2007).

[42] MATLAB, *version 7.10.0 (R2022b)* (The MathWorks Inc., Natick, Massachusetts, 2022).

[43] P. Kollmannsberger, M. Kerschnitzki, F. Repp, W. Wagermaier, R. Weinkamer, and P. Fratzl, The small world of osteocytes: connectomics of the lacuno-canalicular network in bone, New journal of physics **19**, 73019 (2017).

[44] C. Tien, B. Ramarao, and R. Yasarla, A blocking model of membrane filtration, Chemical engineering science **111**, 421 (2014).

[45] K.-J. Hwang and H.-C. Liu, Cross-flow microfiltration of aggregated submicron particles, Journal of membrane science **201**, 137 (2002).